Dalton Transactions

PAPER

View Article Online
View Journal | View Issue

CrossMark click for updates

Cite this: *Dalton Trans.*, 2016, **45**, 6650

Structure and activity of the anticaking agent iron(III) *meso*-tartrate

Arno A. C. Bode,[a] Sanne J. C. Granneman,[a] Martin C. Feiters,[a] Paul Verwer,[b] Shanfeng Jiang,[b] Jan A. M. Meijer,[b] Willem J. P. van Enckevort*[a] and Elias Vlieg[a]

Received 8th January 2016,
Accepted 29th February 2016

DOI: 10.1039/c6dt00098c

www.rsc.org/dalton

Iron(III) *meso*-tartrate, a metal–organic complex, is a new anticaking agent for sodium chloride. A molecular structure in solution is proposed, based on a combination of experimental and molecular modelling results. We show that the active complex is a binuclear iron(III) complex with two bridging *meso*-tartrate ligands. The iron atoms are antiferromagnetically coupled, resulting in a reduced paramagnetic nature of the solution. In solution, a water molecule coordinates to each iron atom as a sixth ligand, resulting in an octahedral symmetry around each iron atom. When the water molecule is removed, a flat and charged site is exposed, matching the charge distribution of the {100} sodium chloride crystal surface. This charge distribution is also found in the iron(III) citrate complex, another anticaking agent. This gives a possible adsorption geometry on the crystal surface, which in turn explains the anticaking activity of the iron(III) *meso*-tartrate complex.

Introduction

Sodium chloride (NaCl, rock salt) is a very important base compound for the chemical industry, which is mainly used for the production of chlorine by electrolysis. Therefore, it is produced and transported in vast quantities. Because it is highly hygroscopic, NaCl is prone to caking, which is prevented using anticaking agents.[1,2]

The most commonly used anticaking agents for NaCl are sodium or potassium ferrocyanide ($[Fe(CN)_6]^{4-}$, hexacyanoferrate(II)) salts. These are very effective in preventing caking, requiring only extremely low concentrations of typically a few parts per million.[3,4] However, ferrocyanide causes problems during electrolysis and it is difficult to remove in advance. Since ferrocyanide contains nitrogen atoms, it causes the formation of nitrogen trichloride (NCl_3, an explosive gas) and the iron atoms are deposited in the form of iron hydroxide on the membranes and electrodes, increasing power consumption. Therefore, a new anticaking agent was required.

Iron(III) *meso*-tartrate (Fe-mTA) was introduced as an alternative anticaking agent for NaCl. It is effective at the same concentrations as ferrocyanide, namely a few parts per million.[5] Since Fe-mTA does not contain nitrogen, no nitrogen trichloride is formed from it during electrolysis. Also, the iron can easily be removed prior to electrolysis, by adding lye. Fe-mTA is only effective as an anticaking agent around pH 4–5.

Recently, we showed how both ferrocyanide and Fe-mTA prevent caking. Both agents are able to inhibit crystal growth of sodium chloride by step pinning.[6] Inhibiting crystal growth prevents caking, because the agglomeration of particles is caused by the slight dissolution and consecutive recrystallisation of the material during humidity cycling of the environment. Furthermore, we showed how the ferrocyanide ion is adsorbed onto the sodium chloride crystal surface,[7] thereby explaining how the ferrocyanide ion pins steps.

For Fe-mTA the mechanism for molecular adsorption on the sodium chloride crystal surface is unknown. Not even the molecular structure of the complex is known, though a structure has been proposed without any experimental evidence.[8] However, knowledge of the molecular structure is required to understand the molecular adsorption geometry of Fe-mTA on sodium chloride.

Our goal is to solve the molecular structure of the anticaking agent Fe-mTA and to understand its interaction with the sodium chloride crystal. From the literature it is known that trivalent metal–tartrate complexes are mostly binuclear and that the carboxyl and hydroxy groups of the tartrate ligands are completely deprotonated,[9–13] in contrast to divalent metal–tartrate complexes.[14,15] A binuclear tartrate complex was suggested for iron(III) D-tartrate.[16] The structure of a binuclear metal *meso*-tartrate was determined for chromium(III),[17] showing that the formation of binuclear complexes is in principle also possible with *meso*-tartrate ligands, as was shown earlier for LD and L complexes.

[a]*Radboud University Nijmegen, Institute for Molecules and Materials, Heyendaalseweg 135, 6525 AJ Nijmegen, The Netherlands. E-mail: W.vanEnckevort@science.ru.nl; Tel: +31 243653433*
[b]*AkzoNobel Industrial Chemicals, Salts and Crystallization, Deventer, The Netherlands*

Iron(III)–tartrates are notoriously difficult to crystallise,[18] only one crystal structure of an iron(III) tartrate is known[19] with racemic (LD) tartrate ions, but this structure is not relevant for the molecular structure in solution and it is not included in the Cambridge Structural Database (CSD). Crystallisation experiments performed in our lab did not produce any single crystals or crystalline powders of Fe-mTA either, only amorphic powders or gels were obtained. Therefore, we studied Fe-mTA in solution combining electron paramagnetic resonance (EPR, also known as electron spin resonance, ESR), UV–VIS spectroscopy, magnetic susceptibility data and molecular modelling techniques. Nuclear Magnetic Resonance (NMR) spectroscopy was not applied, since unpaired electrons broaden NMR signals, usually making NMR unsuitable for paramagnetic systems.[20] We compare our data on Fe-mTA to iron(III) citrate (Fe-citrate), which is also an anticaking agent for sodium chloride, of which the molecular structure and magnetic properties are known.[21,22] Based on all this information, a structure for the complex is proposed together with a possible adsorption geometry of this complex on the sodium chloride {100} crystal surface.

Furthermore, we show that Fe-mTA is a binuclear complex at the pH-range of 4–7, *i.e.* the range at which it is an effective anti-caking agent. At a lower pH, a mononuclear complex is formed, while at a higher pH iron hydroxide is formed.

Experimental

The magnetic properties of the various complexes in solution were studied by measuring the magnetic susceptibility to determine whether the complex is mononuclear or binuclear. In order to get more information on the complexation, the solutions were also studied using UV-VIS spectroscopy and molecular information about the complexes was obtained using EPR. In addition, a single crystal of Fe-citrate was grown with pyridinium as counter ion, in order to check the structure obtained by Shweky *et al.*[21] A single crystal was mounted in air on a glass fibre. Intensity data were collected at −65 °C. A Nonius KappaCCD single-crystal diffractometer was used (phi and omega scan mode) using graphite monochromated Mo-Kα radiation. Intensity data were corrected for Lorentz and polarisation effects. SADABS multiscan correction was applied.[23] The structure was refined with standard methods using SHELXL97.[24]

Aqueous solutions of Fe-mTA, Fe-LTA, Fe-LDTA and Fe-citrate were prepared at various pH-values, by dissolving equimolar amounts of iron(III) chloride ($FeCl_3$) and *meso*-, L- or LD-tartaric acid ($C_4O_6H_6$) or trisodium citrate ($Na_3C_6O_7H_5$) in MilliQ-grade water. As a reference, aqueous iron(III) chloride solutions without ligands were prepared at various pH-values. The pH was set by adding hydrochloric acid or sodium hydroxide.

For the magnetic susceptibility measurements, the concentration used was approximately 0.2 mol L^{-1}. The magnetic susceptibility measurements were performed using a Sherwood Scientific Magnetic Susceptibility Balance. UV-VIS spectra were obtained using a PerkinElmer Lambda 35 UV/VIS spectrometer. The concentration used was approximately 1×10^{-3} mol L^{-1}. The above mentioned measurements were performed at room temperature. The EPR-spectra were recorded using a Bruker ER220 X-band spectrometer at 4.2 K. For the EPR measurements 0.01 mol L^{-1} solutions were prepared. Both the UV–VIS and magnetic susceptibility measurements were corrected for solvent influence by subtracting a clean signal. Diamagnetic corrections were performed for the magnetic susceptibility measurements. The magnetic susceptibility was also measured in saturated sodium chloride solutions. The exact concentrations, after pH calibration, were determined using inductively coupled plasma mass spectroscopy (ICP-MS).

EPR data were recorded for Fe-mTA, Fe-LTA, Fe-LDTA around pH 4.5, and for Fe-mTA and Fe-citrate around pH 2, 4 and 6. The UV-VIS spectra and the magnetic susceptibility were obtained for Fe-mTA and Fe-citrate from pH −1 to 8, for $FeCl_3$ from pH −1 to 7 and for Fe-LTA and Fe-LDTA at pH 0 and pH 4.5.

Molecular modelling used the structure proposed for Fe-mTA[8] as a starting point, since this binuclear structure is a possible fit to our experimental results. The Dmol quantum chemical program as available in the Materials Studio software[25] was used to optimize the complex both in gas phase and in solution, employing a continuum dielectric model.

Results and discussion

Since the Fe-mTA complex did not crystallise, information about the structure of this complex is obtained using various techniques. Fe-mTA is compared to Fe-citrate, which is also an effective anticaking agent for sodium chloride[5] and citrate is a comparable ligand in the sense that it has four deprotonatable (–COOH and –OH) groups. The structure and magnetic properties of the Fe-citrate complex are known.[21,22] The experimental data are used to test a proposed structure for Fe-mTA,[8] which is similar in structure to Fe-citrate. In addition, we compare our data on Fe-mTA and Fe-citrate to the enantiopure Fe-LTA and the racemic Fe-LDTA, which have somewhat weaker anticaking effects.

Single crystal X-ray diffraction

The structure found by Shweky *et al.*[21] was checked using single crystal X-ray diffraction. Fig. 1 shows the obtained crystal structure of Fe-citrate with pyridinium as a counter ion, which is identical to the structure found in the literature. The Fe-citrate structure clearly shows a 2 : 2 binuclear complex, with two iron(III) ions and two bridging, completely deprotonated citrate ligands. Each carboxylate group is coordinated to an iron ion, while the deprotonated hydroxyl group coordinates to both iron ions, forming a bridge. Each iron ion therefore has three coordinating carboxylate groups and two deprotonated hydroxyl groups as ligands. A water molecule coordinates to each iron ion as a sixth ligand, resulting in a

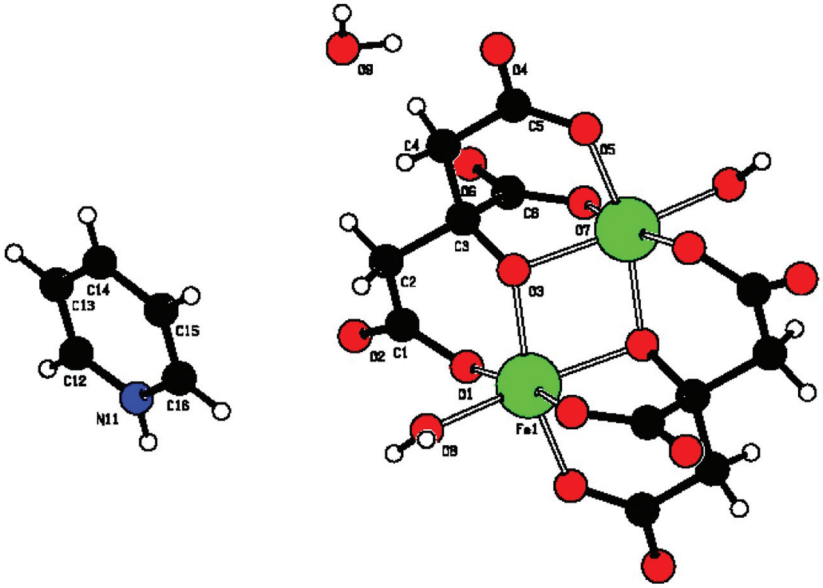

Fig. 1 The crystal structure of Fe-citrate with pyridinium as counter ion. The structure is identical to the one obtained by Shweky *et al.*[21] The 2 : 2 binuclear complex is clearly visible. The citrate ligand is completely deprotonated, including the hydroxy-group, which coordinates to both iron ions, forming a bridge. This bridging explains the antiferromagnetic coupling.

favourable octahedral environment of the iron ion. The two octahedrons are edge-shared, explaining the antiferromagnetic coupling of the iron ions.[22,26] Antiferromagnetic coupling is very common in bridged, binuclear metal complexes, while ferromagnetic coupling is rare and requires precise ligand design.[27,28]

Magnetic susceptibility

The magnetic susceptibility was measured for the iron tartrates and iron citrate to test whether the iron tartrate complexes also show antiferromagnetic coupling. Fig. 2 shows the molar magnetic susceptibility (χ_m in SI units, $cm^3\ mol^{-1}$) as a function of pH for all iron tartrates and iron citrate solutions, both in water and in saturated brine. There is a clear transition between low and higher pH for Fe-mTA: at low pH the magnetic susceptibility of Fe-mTA is quite high, indicating that the iron ions are not antiferromagnetically coupled. At higher pH, the magnetic susceptibility drops, even though the solutions remain clear: no iron hydroxide is formed. This indicates the formation of an antiferromagnetically coupled binuclear complex. Thus there is a change in structure around pH 4. This corresponds well to the fact that Fe-mTA is a good anti-caking agent at pH 4–5, while it is inactive at low pH. At pH 0 and −1, the magnetic susceptibility also decreases, especially in water, an observation that we cannot easily explain. The same trend is observed both in brine and in water, indicating that sodium chloride does not influence the complexation.

The influence of the pH is not as strong for Fe-citrate as for Fe-mTA in water solution, so this Fe-citrate complex is probably more stable at very low pH as will be elucidated further in

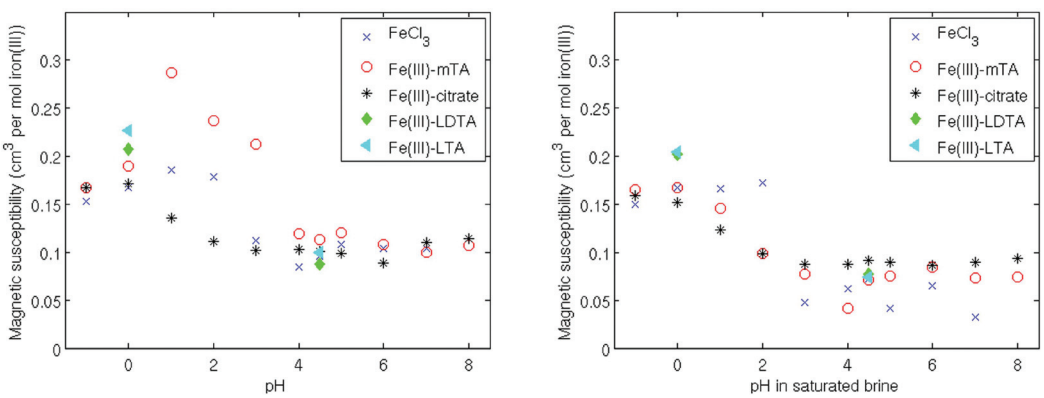

Fig. 2 The molar magnetic susceptibility (χ_m) of Fe-mTA, Fe-citrate and $FeCl_3$ at pH −1 to 7 or 8, and Fe-LTA and Fe-LDTA at pH 0 and 4.5. Left: in water. Right: in saturated brine.

the section on EPR measurements. The magnetic susceptibility is relatively low, so probably the iron ions in the Fe-citrate complex are also antiferromagnetically coupled. Iron chloride has a high χ_m at pH 2 and lower. At pH 3 and higher, χ_m drops, which is readily explained by the formation of iron hydroxide, as confirmed by the fact that the solution becomes turbid.

Interestingly, Fe-LTA and Fe-LDTA show the same magnetic behaviour as Fe-mTA: at low pH the magnetic susceptibility is high, indicating no antiferromagnetic coupling, while at pH 4.5, the magnetic susceptibility is lower even though there is no iron hydroxide formation. Therefore we assume that also L- and LD-tartrate iron(III) complexes are binuclear and antiferromagnetically coupled at pH 4.5, which is in agreement with results obtained by Timberlake.[16] So, these complexes are also binuclear, and they are anticaking agents as well, although weaker than Fe-mTA.[2] A possible explanation for this is given in the section on modelling.

The spin quantum number S ($S = \frac{1}{2}N$, N = number of unpaired electrons) of the iron ions was calculated to test whether the transition at pH 4 can be attributed to the formation of binuclear complexes at pH above 4. The spin state of mononuclear complexes should be similar to that of free iron(III) ions, since antiferromagnetic coupling is not possible. The spin quantum number can be calculated from the molar magnetic susceptibility (χ_m) of the solutions, applying diamagnetic corrections for the ions present.[29] The effective magnetic moment, μ_{eff} expressed in Bohr magnetons (μ_B), depends on χ_m as follows:

$$\mu_{eff} = \sqrt{\frac{3k_bT\chi_m}{N_A{\mu_0}{\mu_B}^2}}, \quad (1)$$

in which k_b is the Boltzmann constant, T the temperature in Kelvin, N_A the Avogadro constant and μ_B the Bohr magneton. The magnetic moment of the iron atoms, $\mu_{spin\ only}$, is usually the main contribution to the effective magnetic moment of the entire molecule, so

$$\mu_{eff} \cong \mu_{spin\ only}. \quad (2)$$

Subsequently, $\mu_{spin\ only}$ only depends on the spin quantum number S of the iron ions as:

$$\mu_{spin\ only} = g_e\sqrt{S(S+1)}, \quad (3)$$

in which g_e is the electron g-factor. The high values for χ_m around pH −1 to 3 are approximately 0.17 $cm^3\ mol^{-1}$, corresponding to an effective magnetic moment of $5.7\mu_B$ and a high spin quantum number S of 2.4. This value is in good agreement with the spin quantum number for free iron(III) atoms, S = 5/2, indicating that at this pH range the complexes are mononuclear, in contrast to the high pH range. The highest values for χ_m, around 0.28 $cm^3\ mol^{-1}$, are probably due to other contributions to the magnetic moment next to the spin, like orbital contributions, making the assumption in eqn (2) invalid.

Optical observations and UV–VIS spectroscopy

Colour transitions in solutions of metal complexes are indications of structure transitions of the complexes involved and therefore they should correspond to the transitions detected using the magnetic susceptibility. The colours of the iron tartrate and iron citrate solutions in water vary strongly with the pH. However, the colour of the solutions did not depend on the solute concentration, therefore the complexation does not change strongly with the concentration. The colours of the solutions were identical in saturated brine. The solutions of all complexes are orange at pH −1 and are yellow at pH 0 and 1. In the pH-regime from 3 to 5, Fe-mTA solutions turn green. This interval corresponds to the regime in which this complex is an active anticaking agent. At higher pH, from 6 to 8, the Fe-mTA solutions turn brownish to red though they remain clear, probably due to the formation of iron hydroxide clusters.

A similar trend is observed for Fe-citrate: from pH −1 to 1 the solutions are yellow; from pH 2 to 4, the solution turns from red to greenish, and at higher pH values, the solutions turn red. Fe-LTA and Fe-LDTA are not green around pH 4.5, but red. The green colour is probably typical for iron(III) complexes which have the right iron environment for optimal anticaking activity, since the green colour is observed for both Fe-mTA and Fe-citrate in the pH range at which they are active anticaking agents. $FeCl_3$ behaves very differently at pH 3 and upwards, turning brownish turbid due to the precipitation of iron hydroxide. Photographs of the solutions in saturated brine are given in the Appendix.

The complexation of the iron tartrates and citrate in aqueous solution was also studied using UV–VIS, to show that the mononuclear complexes disappear at a pH above 3. Mononuclear complexes of these compounds have a characteristic absorption at 300–400 nm.[16] In Fig. 3 the UV-VIS absorbance spectra of all solutions at low concentrations are shown. The absorbance at wavelength λ, A_λ, is plotted against this wavelength. A_λ is defined as

$$A_\lambda = -^{10}\log\left(\frac{I}{I_0}\right), \quad (4)$$

in which I is the transmitted intensity and I_0 is the incident intensity at wavelength λ. At 225–250 and 300–400 nm a broad peak is observed for both Fe-citrate and Fe-mTA at pH −1 to 1 (top left and top right figures). At pH 2 and 3, weak traces of these peaks can be seen, and the peaks are not present at higher pH values. Iron(III) chloride also shows a peak in absorbance in the 300 to 400 nm regime at pH −1 to 2 (bottom left). At pH 3 the peak is no longer visible and at higher pH values, the total absorbance decreases due to precipitation of iron hydroxide. Also for Fe-LTA and Fe-LDTA (bottom right), a clear peak at 300–400 nm is observed at pH 0. The peak at 300–400 nm indicates a mononuclear complex,[16] having no antiferromagnetic coupling. This peak disappears at the high pH-ranges at which the complexes show a lowered magnetic susceptibility, further proof of a structure transition of the complex.

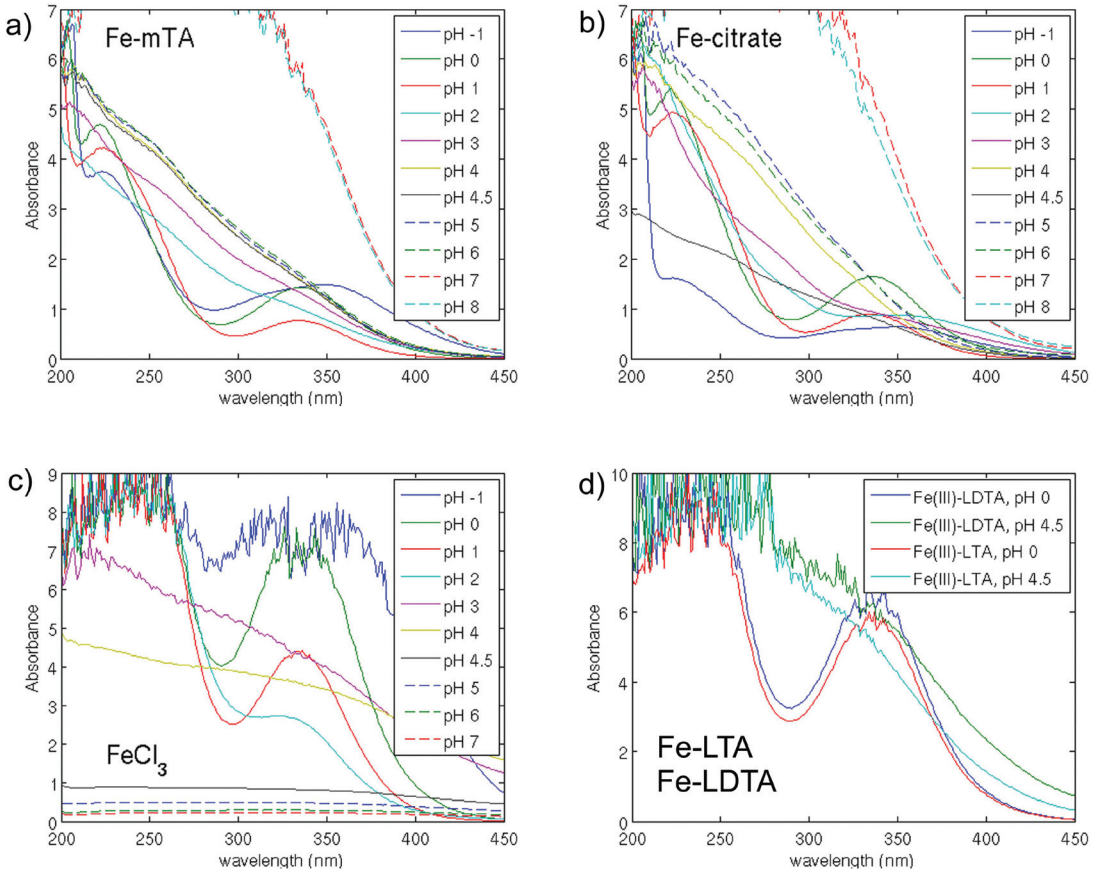

Fig. 3 UV-VIS spectra of the iron(III) tartrates, iron(III) citrates and iron(III) chloride at pH –1 to 7 or 8. (a) Fe-mTA, (b) Fe-citrate, (c) $FeCl_3$ and (d) Fe-LTA and Fe-LDTA, at pH 0 and 4.5. The spectra are "noisy" for absorbances >7, due to the detection limit of the spectrometer. Similar results were obtained for saturated brine as a solvent.

EPR measurements

Fig. 4 shows the EPR spectra of the complex solutions in water. All spectra have as the most important feature a signal around 1600 Gauss (1 Gauss = 10^{-4} Tesla) $g = 4.3$), which indicates the presence of high-spin Fe(III) ($S = 5/2$) with a high rhombicity. The signals in the region around 3000 Gauss, *i.e.* the sharp radical-like signal at 3200 Gauss ($g = 2$) and the copper(II) impurity signal in Fig. 4c at 3000 Gauss, are background signals which can be ignored for the discussion.

It is difficult to compare the intensity of the EPR signals, as estimated from the amplitude at $g = 4.3$, of the three data sets (in Fig. 4a–c). This can be seen from the different intensities though identical shapes of the signals of Fe-mTA at pH 4.4 and 4.2 in Fig. 4a and b respectively. Probably this is due to different sample alignment or preparation: all signals in Fig. 4b are relatively weak. However, within each data set comparisons can be made. In Fig. 4b, the signal from Fe-mTA at pH 1.7 is relatively strong, compared to Fe-mTA at pH 4.2 and 6.9. These weaker signals at pH 4.2 and 6.9 probably originate from antiferromagnetically coupled complexes, which therefore are almost EPR silent. In contrast, the relatively strong signal from Fe(III)-mTA at pH 1.7 originates from mononuclear complexes, which do not show antiferromagnetic coupling. Therefore, this signal is more intense. The intensity of the iron citrate samples is independent of the pH between pH 2.3 and 6.0 (see Fig. 4c).

These results are consistent with the magnetic susceptibility measurements in water (Fig. 2, left), from which it was concluded that the antiferromagnetic coupling of the Fe-mTA was broken at pH 3 and below, whereas that of the Fe-citrate was still stable at pH 2. This can be explained by the pK_a values of the ligands, since protonation of a ligand will destabilise the binuclear complexes, and the pK_a value of a –OH group is much higher than that of a –COOH group. It can be expected that at low pH a tartrate ligand is more easily protonated than a citrate ligand: a tartrate ligand has two deprotonated hydroxy groups and two carboxylate groups, whereas a citrate ligand has three carboxylate groups and only one deprotonated hydroxy group. So both the iron tartrate and the iron citrate complexes show antiferromagnetic coupling, however at a slightly different pH range.

The spectra of Fe-mTA at pH 4.4 and 4.2, in Fig. 4a and b respectively, contain an additional very broad signal that is approximately centred around $g = 2$ and of which the origin is unknown.

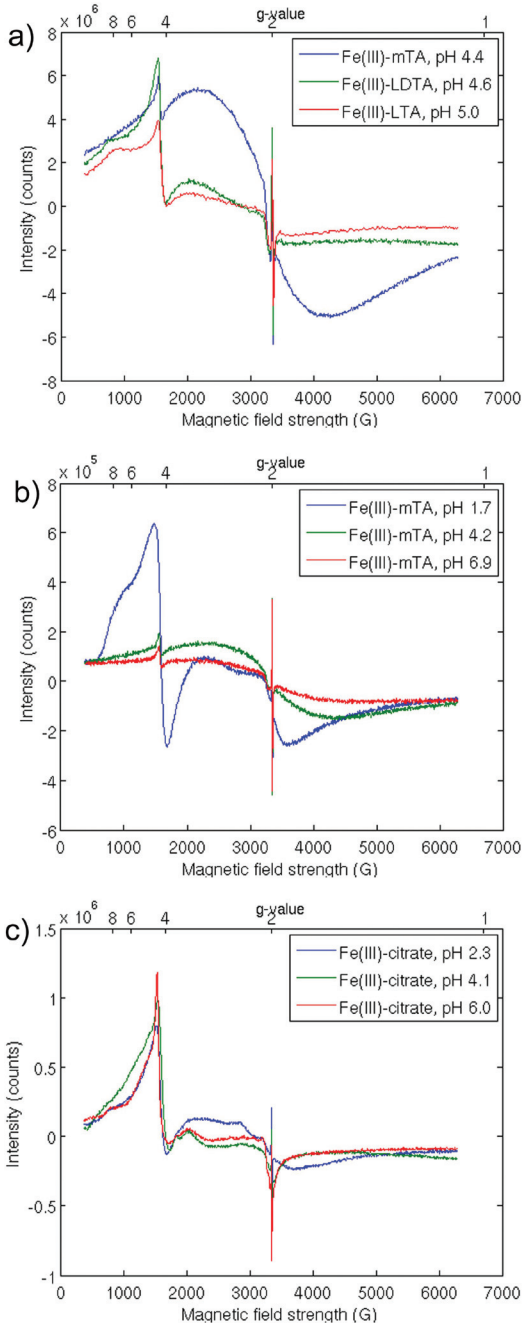

Fig. 4 EPR spectra of aqueous solutions of iron(III)–tartrates and iron(III)–citrates. (a) Fe-mTA, Fe-LTA and Fe-LDTA at pH 4.5–5. (b) Fe-mTA at pH 1.7, 4.2 and 6.9. (c) Fe-citrate at pH 2.3, 4.1 and 6.0.

Fig. 4a shows the spectra of Fe-mTA, Fe-LTA and Fe-LDTA at pH values in the range 4.5–5. It can be seen that the environment of the iron in the Fe-LTA and Fe-LDTA complexes is different from that in the Fe-mTA complex, since there is a shoulder at g = 8–10, which is not present in the Fe-mTA spectrum. In Fig. 4b, the spectrum of Fe-mTA at pH 1.7 has a similar shoulder at g = 8–10, indicating that the iron environment is different from that at pH 4.2 and 6.9, and is probably similar to the iron environments in the Fe-LTA and Fe-LDTA complexes at pH 4.5–5 (Fig. 4a). These shoulders indicate a somewhat lower rhombicity of the iron environment compared to the Fe-mTA complex at pH 4.2–6.9.[30] So, the lower rhombicity in the iron tartrate complexes correlates with inactivity or reduced activity as an anticaking agent (Fe-mTA at pH 1.7 and Fe-LTA and Fe-LDTA at pH 4.5–5).

For the Fe-citrate spectra in Fig. 4c, the signal does not change drastically between pH 2.3 and 6, except for the higher intensity at g = 4.3–10 at pH 4.1, so the environment of the iron ion has a little lower rhombicity at this pH.[30] All magnetic fields and corresponding g values for the signals observed on the low-field side of the g = 4.3 signal fall within the range observed for a rhombogram calculated for S = 5/2 systems,[30] so all signals can be explained as due to high-spin iron(III) with subtly different environments and the oxidation state of the iron atoms is not changed.

Molecular modelling of the Fe-mTA complex

A geometry optimization using quantum chemical methods is performed on the Fe-mTA complex structure proposed by Geertman[8] (see Fig. 5a). The pH cannot be explicitly modelled, so the tartrate ligands are modelled as completely deprotonated at pH 4.5, based on the iron citrate crystal structure and the literature.[9–13] Furthermore, the Fe-mTA structure shows antiferromagnetic coupling and therefore it is a binuclear complex at this pH. This is in agreement with the proposed molecular structure.

The Dmol quantum chemical program as available in the Materials Studio software[25] was used to optimize the complex (which has a net charge of −2) both in vacuum (gas phase) and placed in a continuum with a dielectric constant of 78 to assess the effect of a polarizable environment such as water or brine. The GGA BP potential was used, with a DNP basis set, an octupolar charge density expansion and a 5.5 Å orbital cutoff. The cosmo method was used to create the dielectric environment. Doing the optimization both in gas phase and in a dielectric continuum should give a good idea of the potential effect of the solvent on the optimized structure. In both optimizations, the water molecule in the centre of the proposed complex (Fig. 5a) immediately leaves the structure. The final optimized structure was therefore obtained by optimizing the complex again without this water molecule. Furthermore, the oxygen atoms of the *meso*-tartrate ligands rearrange. This results in the structure shown in 5b. For one *meso*-tartrate ligand, one carboxyl oxygen and one hydroxy oxygen atom coordinate to one iron atom. The second hydroxy group forms a bridge between the two iron atoms, by coordinating to both atoms. The second carboxyl oxygen coordinates only to the second iron atom. This ligand is therefore coordinated to one iron atom with three bonds, and to the other iron atom with two bonds. The other ligand coordinates identically, but is inversed centrosymmetrically. Therefore, each iron atom has five coordinating oxygen atoms from the *meso*-tartrate ligands. Each iron atom is exposed to the outside of the complex, allowing one water molecule to coordinate to each iron atom as a

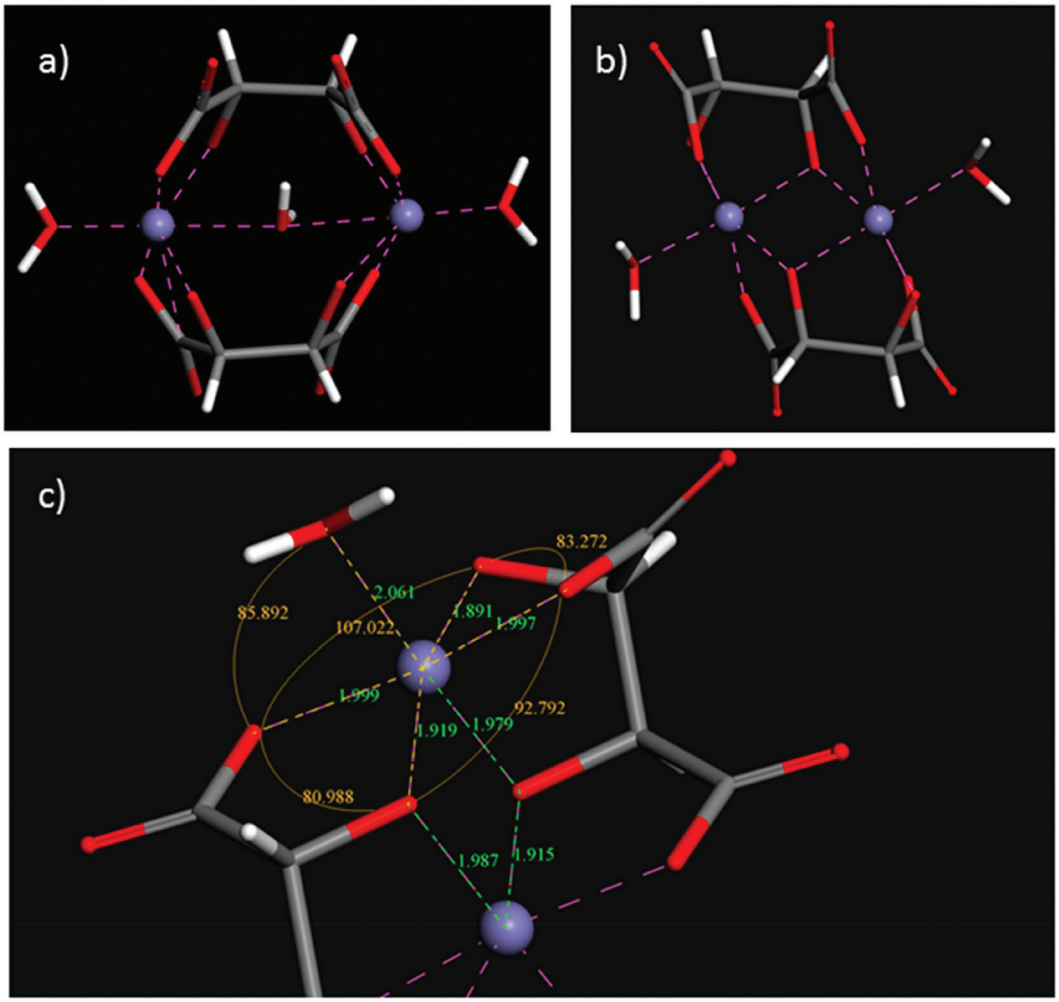

Fig. 5 Subsequent steps in the molecular modelling of the Fe-mTA complex. (a) The initial structure as proposed by Geertman.[8] (b) The structure after minimisation using quantum mechanics and a dielectric of 78. (c) The geometry around the Fe^{3+} ion in the optimized complex. Colour codes in the graphs: grey: carbon, red: oxygen, white: hydrogen, iron: blue.

sixth ligand. Six-fold octahedral coordination is a favourable environment for iron atoms.

Fig. 5c shows the geometrical details of the environment of an iron atom in this complex. The six coordinating oxygen atoms form a distorted octahedron around each iron atom. The O–Fe–O angles vary between 80 and 107° and the Fe–O bond lengths vary from 1.89 to 2.06 Å. The distortion is in agreement with the high rhombicity of the iron environment in Fe-mTA, as was detected using EPR (see Fig. 4). The two octahedrons in the Fe-mTA complex are edge-shared through the bridging deprotonated hydroxy groups, similar to the Fe-citrate complex (compare Fig. 1 and 5b). This explains the antiferromagnetic coupling[26] that was observed in Fig. 2. So, the simulated structure is in excellent agreement with our experimental results.

A suggestion for the adsorption geometry of the Fe-mTA complex on {100} NaCl

Recently, it was shown that the Fe-mTA complex is able to block crystal growth of sodium chloride by pinning the propagation of steps on the NaCl {100} surface.[6] This indicates that this complex is firmly adsorbed on this surface. When studying the structure obtained from molecular modelling, a possible binding mechanism is found. It is based on the observation that the bottom (and top) side of the complex where the water molecule is adsorbed is very flat. When this water molecule is removed, a surface is revealed with the positively charged iron atom at the centre, surrounded by four negatively charged oxygen atoms, as is shown in Fig. 6a. These charges are distributed at roughly 90° angles to each other, resembling the symmetry of the {100} NaCl surface. This gives a fivefold coordination of the iron with a square-pyramidal geometry, with a square planar configuration of the four oxygen atoms at its under-surface.

We therefore propose that the water molecule of the Fe-mTA complex desorbs, and subsequently the iron atom coordinates to the NaCl surface above a chloride ion. The surrounding oxygen atoms will coordinate to the sodium ions adjacent to the chloride ion. This adsorption geometry is shown in

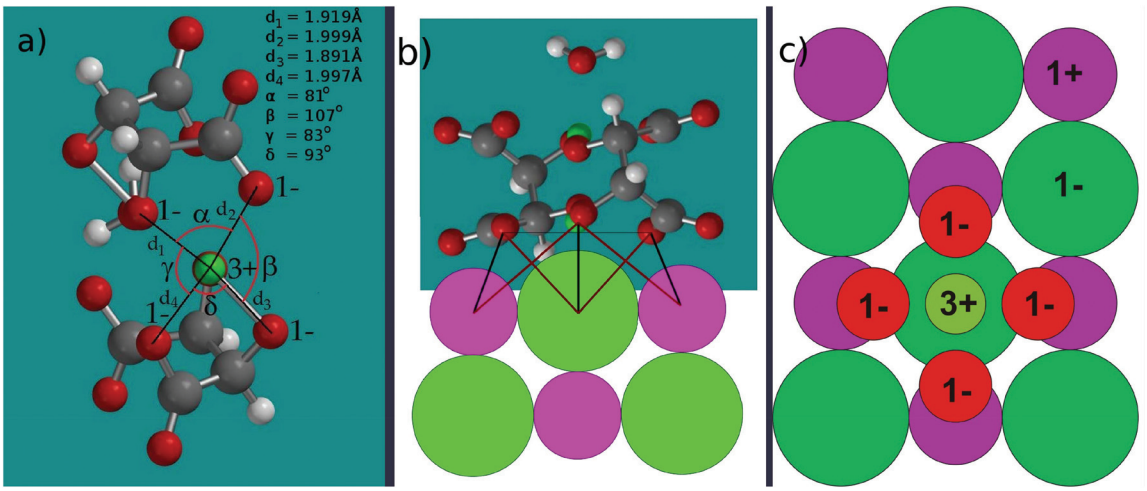

Fig. 6 The proposed adsorption geometry. The Fe-mTA complex shown in Fig. 5c is very flat when the water molecule is removed. (a) Removal of the water molecule reveals a highly charged site. The negative oxygen charges are almost at right angles and the distances from the central positive Fe^{3+} ion are approximately 2 Å. This charge distribution may allow adsorption onto the sodium chloride {100} surface, of which the angles Na–Cl–Na are 90° and the Na–Cl distances are 2.8 Å. (b) Side view of the proposed adsorption geometry. (c) Top view of this geometry, only showing the NaCl surface and the iron and oxygen atoms involved in the adsorption. Colour codes in the graphs: grey: carbon, red: oxygen, white: hydrogen, small green: iron, purple: sodium and large green atoms: chloride.

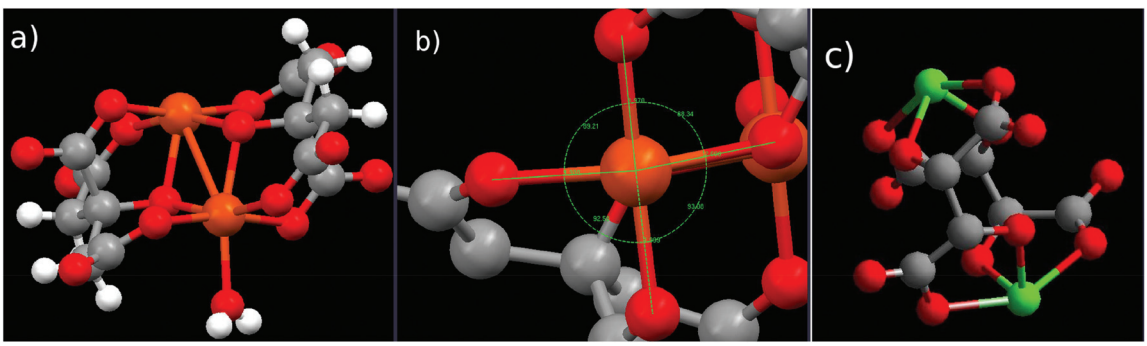

Fig. 7 Other binuclear complexes to be compared with the Fe-mTA structure of Fig. 5 and 6. (a) Flat side of the Fe-citrate complex, comparable to Fig. 6b and c prior to the removal of the water molecule. Though a part sticks out, the iron site is exposed and should be able to attach to the NaCl {100} surface, especially at step sites. (b) Expanded view of the coordination site in the Fe-citrate complex. The structure is very similar to Fig. 6a. Fe–O bond lengths are 1.97–2.00 Å and the angles are 88–93° (c) Binuclear complex of antimony with LD-tartrate.[9] This complex does not have bridging oxygen atoms and the metal atoms stick out. The Fe-LDTA and Fe-LTA complexes are expected to be very similar. Colour codes: grey: carbon, red: oxygen, white: hydrogen, orange: iron and green: antimony.

Fig. 6b and c. Another argument for this adsorption geometry is that the Fe-citrate complex, which is also an active anti-caking agent, has a very similar charge distribution when the adsorbed water molecule is removed, as is shown in Fig. 7a and b. Thus the adsorption geometry of the Fe-citrate complex is probably similar to the adsorption geometry proposed for the Fe-mTA complex.

For the proposed geometry to work, one water molecule has to be removed from the Fe-mTA complex. Furthermore, four water molecules have to be removed from the sodium chloride crystal surface, since there is one water molecule adsorbed onto each sodium ion on the clean sodium chloride {100} surface at high humidity.[31] Energetically this is favourable, since an electrostatic Madelung calculation showed that the bonding energy between the complex and the surface is in the order of 2000 kJ mol^{-1}. In contrast, the bonding energy of a water molecule to an iron(III) ion is approximately 170 kJ mol^{-1} (ref. 32) and the bonding energy of a water molecule on a sodium chloride crystal is also approximately 170 kJ mol^{-1}.[33]

Fe-LTA and Fe-LDTA

Fig. 7c shows the crystal structure of a binuclear antimony LD-tartrate complex.[9] It is likely that the Fe-LTA and Fe-LDTA complexes are similar to this compound. This structure does not

have bridging oxygen atoms and the metal atoms stick out. This complex does not show the square-pyramidal structure like Fe-mTA and Fe-citrate, as shown in Fig. 6b and 7b. This possibly explains why both Fe-LTA and Fe-LDTA are less active as anticaking agents for sodium chloride, as compared to Fe-mTA and Fe-citrate.[2]

Conclusion

From our experiments and simulations we can conclude that the active anticaking agents Fe-mTA and Fe-citrate are both binuclear high spin iron(III) complexes, bridged by deprotonated hydroxy groups from their corresponding ligands. Simulation results based on this structure suggest that a square-pyramidal coordination symmetry around the iron atom is typical for the anticaking activity of these complexes, since this geometry allows for adsorption to the NaCl {100} surface. In addition, the results show that the less active iron tartrate complexes (Fe-LTA and Fe-LDTA) are also binuclear complexes, though the EPR experiments and comparison with the literature indicate that their internal structure is different, possibly lacking the bridging hydroxyl groups and square-pyramidal coordination symmetry.

Appendix

Solutions of complexes in saturated brine. Top row: Fe(III)-mTA at pH −1 to 8. Second row: Fe(III)-citrate at pH −1 to 8. Third row: Fe(III) chloride at pH −1 to 7. Bottom row: Fe(III)-LTA (left) and Fe(III)-LDTA (right) at pH 0 and 4.5.

Acknowledgements

The authors would like to thank Bas de Bruin and Paul Schlebos for performing the EPR experiments. Furthermore, we would like to acknowledge Paul Tinnemans for determining the iron(II)-mTA crystal structure, Jan Smits for the determination of the iron(III)-citrate crystal structure, Jelle Eygensteyn for performing the ICP-MS measurements and Rob Geertman for fruitful discussions. Finally, the authors acknowledge Akzo Nobel Industrial Chemicals and the Dutch Ministry of Economic Affairs for funding (EOS-KTO program, AgentschapNL).

References

1 D. W. Kaufmann, *Sodium Chloride: the production and properties of salt and brine*, Reinhold, 1960.
2 A. A. C. Bode, M. Verschuren, M. Jansen, S. Jiang, J. A. M. Meijer, W. J. P. van Enckevort and E. Vlieg, *Powder Technol.*, 2015, **277**, 262–267.
3 M. A. van Damme-van Weele, *Influence of additives on the growth and dissolution of sodium chloride crystal*, PhD thesis, Technische Hogeschool Twente, Enschede, 1965. See also: M. A. M. van Damme-van Weele, The influence of ferrocyanide complexes on the dissolution of sodium chloride, in *Adsorption et Croissance Crystalline*, ed. R. Kern, Coll. CNRS, 1965, vol. 152, pp. 433–449.
4 R. Boistelle, *Contribution à la connaissance des formes de croissance du chlorure de sodium*, PhD thesis, Université de Nancy, 1966. See also: M. Bienfait, R. Boistelle and R. Kern, Les morphodromes de NaCl en solution et l'adsorption d'ions étrangers, in *Adsorption et Croissance Crystalline*, ed. R. Kern, Coll. CNRS, 1965, vol. 152, pp. 577–594.
5 R. M. Geertman, Use of carbohydrate-based metal complexes in non-caking salt compositions, *US patent*, WO00/59828, 2006.
6 A. A. C. Bode, S. Jiang, J. A. M. Meijer, W. J. P. van Enckevort and E. Vlieg, *Cryst. Growth Des.*, 2012, **12**, 5889–5896.
7 A. A. C. Bode, V. Vonk, D. J. Kok, F. J. van den Bruele, A. Kerkenaar, M. Mantilla, S. Jiang, J. A. M. Meijer, W. J. P. van Enckevort and E. Vlieg, *Cryst. Growth Des.*, 2012, **12**, 1919–1924.
8 R. M. Geertman, *VDI-Berichte*, 2005, **1901**, 557–562.
9 G. A. Kiosse, N. I. Golovastikov and N. V. Belov, *Proc. Natl. Acad. Sci. USSR*, 1964, **155**, 545.
10 J. G. Forrest and C. K. Prout, *J. Chem. Soc. A*, 1967, **8**, 1312–1317.
11 B. Kamenar, D. Grdenic and C. K. Prout, *Acta Crystallogr., Sect. B: Struct. Crystallogr. Cryst. Chem.*, 1970, **26**, 181–188.
12 R. E. Tapscott, R. L. Belford and I. C. Paul, *Coord. Chem. Rev.*, 1969, **4**, 323–359.
13 R. E. Tapscott, *Inorg. Chim. Acta*, 1974, **10**, 183–189.
14 D. X. Li, D. J. Xu and Y. Z. Xu, *Acta Crystallogr., Sect. E: Struct. Rep. Online*, 2004, **60**, m1982–m1984.

15 In our laboratory, we determined that Fe(II)-mTA is isomorphic to the crystal structure of Co(II)-mTA[12] by matching the XRPD spectrum of Fe(II)-mTA to a calculated XRPD spectrum. This spectrum was calculated from its crystal structure, which was obtained by replacing the cobalt(II) ion by an iron(II) ion in the crystal structure of Co(II)-mTA. The element replacement is justified since Co(II) and Fe(II) are adjacent in the periodic table, are both bivalent and have a comparable ionic radius, (88.8 and 92 pm).
16 C. F. Timberlake, *J. Chem. Soc.*, 1964, **Apr**, 1229–1240.
17 G. L. Robbins and R. E. Tapscott, *Inorg. Chem.*, 1976, **15**, 154–159.
18 M. Bobtelsky and J. Jordan, *J. Am. Chem. Soc.*, 1947, **69**, 2286–2290.
19 M. A. Ivanov and A. L. Kosoy, *Acta Crystallogr., Sect. B: Struct. Crystallogr. Cryst. Chem.*, 1975, **31**, 2843–2848.
20 R. H. Crabtree, *The Organometallic Chemistry of the Transition Metals*, Wiley, Hoboken, NJ, USA, 2005.
21 I. Shweky, A. Bino, D. P. Goldberg and S. J. Lippard, *Inorg. Chem.*, 1994, **33**, 5161–5262.
22 X. Hao, Y. Wei and S. Zhang, *Transition Met. Chem.*, 2001, **26**, 384–387.
23 G. M. Sheldrick, *SADABS Program for Empirical Absorption Correction*, 1996.
24 G. M. Sheldrick, *SHELXL-97. Program for the refinement of crystal structures*, 1997.
25 Accelrys Software Inc., *Materials Studio Modeling Environment, Release 3.1*, Accelrys Software Inc., San Diego, 2004.
26 Y. G. Wei, S. W. Zhang and M. C. Shao, *Polyhedron*, 1997, **16**, 2307–2313.
27 O. Kahn, *Inorg. Chim. Acta*, 1982, **62**, 3–14.
28 O. Kahn, *Angew. Chem., Int. Ed. Engl.*, 1985, **24**, 834–850.
29 C. E. Housecroft and A. G. Sharpe, *Inorganic Chemistry*, Pearson/Prentice Hall, 2nd edn, 2005.
30 W. R. Hagen, *Dalton Trans.*, 2006, 4415–4434.
31 J. Arsic, D. M. Kaminski, N. Radenovic, P. Poodt, W. S. Graswinckel, H. M. Cuppen and E. Vlieg, *J. Chem. Phys.*, 2004, **120**, 9720–9724.
32 M. Rosi and C. W. Bauschlicher Jr., *J. Chem. Phys.*, 1989, **12**, 7264–7272.
33 P. B. Barraclough and P. G. Hall, *Surf. Sci.*, 1974, **46**, 393–417.